Journal of Inorganic and Organometallic Polymers and Materials (2022) 32:3797–3812
https://doi.org/10.1007/s10904-022-02373-2

Evaluation of In Vitro Bioactivity, Cytotoxicity, and Drug Release Behavior of Er_2O_3 and Tb_2O_3-Containing Bioactive Glass Particles and Nanofibers

Begüm Rahman[1] · Aylin M. Deliormanlı[1] · Harika Atmaca[2]

Received: 10 March 2022 / Accepted: 6 May 2022 / Published online: 6 June 2022

Abstract
Silicate-based bioactive glasses doped with Er^{3+} and Tb^{3+} ions (1, 3, and 5 wt%) were synthesized in the form of powders and nanofibers using sol–gel and electrospinning methods, respectively. In vitro bioactivity of the prepared powders and fibers was analyzed in simulated body fluid (SBF) for various periods, and the biological response of the osteoblastic MC3T3-E1 cells to the bioactive glass samples was studied using MTT assay and microscopic observations. The amoxicillin release behavior of the prepared glasses was examined in phosphate-buffered saline as a function of time. The results revealed that the incorporation of Er^{3+} and Tb^{3+} improved the hydroxyapatite forming ability of the prepared bioactive glass samples for up to 30 d of immersion in SBF. In vitro cytotoxicity experiments showed that Tb^{3+}-containing glass samples were biocompatible at all concentrations; however, in the case of Er^{3+}-containing glass particle-based samples, a decrease in cell viability was observed starting from 3 wt% Er^{3+}. SEM observations revealed cellular adhesion and spreading on the bioactive glass scaffolds. Drug delivery experiments demonstrated that after 24 h, ~ 35 to 38% of the drug was released into the medium for both bioactive glass powder and nanofiber-based samples. Bioactive glasses synthesized in the study have the potential to be used in bone tissue engineering applications.

Keywords Bioactive glass · Particle · Nanofiber · Osteoblastic cells · Drug delivery

1 Introduction

A special group of biomaterials used in tissue engineering applications with high specific biological activity when in contact with physiological fluids is bioactive glasses [1]. They are promising materials for tissue engineering, drug delivery, and dental applications owing to their high biocompatibility, bioactivity, and osteoconductivity [1–3]. Crystalline hydroxyapatite (HA) or amorphous calcium phosphate layer, which is chemically similar to the components constituting the bone tissue, is formed when the bioactive glass comes into contact with physiological fluids. Bioactive glasses can integrate with both hard and soft tissues [4–6].

It is known that therapeutic elements are added to the composition of biomaterials to modify or improve their physical and biological properties such as bioactivity and cellular response [7, 8]. For example, rare-earth elements are added to biomaterials to provide photoluminescence properties for bio-imaging applications [9]. Novel glass compositions substituted with different rare-earth elements have been studied by various research groups previously [10–14]. Erbium (Er) is a rare earth element that is naturally present in a rib bone of a healthy human and can be utilized for biomedical applications [15]. Erbium-based lasers have been used in medical and dental practice [16]. Li et al. [17] synthesized bioactive glasses doped with Er^{3+}/Yb^{3+} having luminescence properties. It has been also reported that Er^{3+}/Yb^{3+} doped bioactive glasses are non-toxic and biocompatible with MC3T3-E1 cells. Previously, Pham et al. [18] investigated the light radiation from Er^{3+} doped hydroxyapatite/β-tricalcium phosphate (HA/β-TCP) composites. The formation of Er^{3+}-containing HA/β-TCP samples emerged a considerably enhanced light emission at

✉ Aylin M. Deliormanlı
aylin.deliormanli@cbu.edu.tr

[1] Department of Metallurgical and Materials Engineering, Manisa Celal Bayar University, Yunusemre, Manisa, Turkey

[2] Department of Biology, Manisa Celal Bayar University, Yunusemre, Manisa, Turkey

~ 1540 nm, which has a potential for bio-medicinal usage [18].

Another rare earth element that is used in biomedical applications is terbium (Tb). A radioisotope Tb-149 has been used in targeted cancer therapy [19]. Previously, it has been reported that biomaterials doped with low concentrations of Tb^{3+} can significantly increase the luminescence properties while maintaining the main physicochemical and biological activity [20, 21]. The potential biomedical applications of Tb^{3+}-doped hydroxyapatites were investigated in the past and in vitro cytocompatibility with MC3T3-E1 and A549 cells have been documented [22]. Wang et al. [23] used the sol–gel method to synthesize nanoparticles of mesoporous bioactive glass doped with Tb^{3+} (Tb^{3+} /MBG). The in vitro bioactivity studies of the produced Tb^{3+}/ MBG, kept in SBF for 3 days, showed that the inclusion of Tb^{3+} ions improved the ability of hydroxyapatite formation.

Deliormanlı and colleagues [24] have investigated the structural and photoluminescence properties of Er^{3+} and Tb^{3+}-doped silicate-based 13–93 bioactive glasses in the form of particles and nanofibers. The findings of the study revealed that dopant concentration and sample morphology have a substantial impact on the photoluminescence and HA conversion capabilities of the related bioactive glasses. 13–93 bioactive glasses comprising Er^{3+} and Tb^{3+} have been reported to have the potential to be used in tissue engineering and bio-imaging studies as well as for the development of ionization radiation shielding materials [24, 25]. However, the manufactured bioactive glasses' detailed in vitro bioactivity in SBF, cytotoxicity, and drug release behavior have yet to be investigated. Therefore, this study aims to examine the in vitro HA forming ability of Er^{3+} and Tb^{3+}-doped 13–93 bioactive glasses and evaluate their cytotoxicity using the osteoblastic MC3T3-E1 cell line and the drug release behavior using a well-known antibiotic utilized in the treatment of bone infections.

2 Experimental Studies

2.1 Powder Synthesis

The sol–gel process was used to synthesize Er^{3+} and Tb^{3+}-containing 13–93 bioactive glass particles. Table 1 shows the chemical composition (in weight percent) of the bioactive glasses examined. The method used in sol–gel synthesis has been described elsewhere [24, 25]. For the particle synthesis, a specific amount of TEOS (Sigma-Aldrich, Germany) was added to a 0.3 M HNO_3 solution at 25 °C and agitated for 60 min to allow for hydrolysis. Then, in a 15-min interval, the other ingredients [$(C_2H_5O)_3PO$, $Ca(NO_3)_2{\cdot}4\ H_2O$, $Mg(NO_3)_2{\cdot}6H_2O$, $NaNO_3$, KNO_3 (all from Sigma-Aldrich, Germany)] were added, and the complete solution was stirred for another 30 min. In addition, for the synthesis of the rare-earth element-doped samples, 13–93 glass solutions contained specified concentrations of $Er(NO_3)_3.5H_2O$ and/or $Tb(NO_3)_3.5H_2O$ (at 1, 3, or 5 wt%). The final transparent solution was agitated overnight, and the resulting glass solution was kept at 25 °C in a closed bottle for gel formation. The gel network was aged at 60 °C for 48 h after 5 days of gelation before being dried at 120 °C for 24 h. A heat treatment at 625 °C for 4 h at a heating rate of 5 °C/min was used to remove the organic components and nitrates. The calcined particles were reduced in size using a high-speed planetary micro mill (Fritch, Pulverisette 7, Premium Line, Germany) rotating at 700 rpm for 10 min.

2.2 Nanofiber Synthesis by Electrospinning

The electrospinning method was used to prepare Er^{3+} and Tb^{3+}-containing 13–93 bioactive glass nanofibers. The fabrication procedure for the glass fibers was previously described in detail [24, 26]. After preparing the bioactive glass solution as described above, an aqueous poly (vinyl

Table 1 Composition (wt%) of the bioactive glass formulations studied

Sample	SiO_2	CaO	Na_2O	K_2O	MgO	P_2O_5	Er_2O_3	Tb_2O_3
1393 (BG)	53	20	6	12	5	4	-	-
1Er-BG	52	20	6	12	5	4	1	-
3Er-BG	50	20	6	12	5	4	3	-
5Er-BG	48	20	6	12	5	4	5	-
1 Tb-BG	52	20	6	12	5	4	-	1
3 Tb-BG	50	20	6	12	5	4	-	3
5 Tb-BG	48	20	6	12	5	4	-	5

alcohol) (PVA, Alfa Aesar, 87–89% hydrolyzed, high molecular weight) solution (10 vol.%) was added to the glass (at a 1:1 ratio). Before the electrospinning procedure, the resulting solution was agitated for 3 h at 25 °C for homogenization. Electrospinning equipment (NE-300, Inovenso, TR) was utilized to fabricate erbium and terbium-containing glass nanofibers. A syringe pump was used to deliver the bioactive glass-PVA solution at a rate of 0.5 mL/h into a stainless steel nozzle with a diameter of 0.8 mm. As the target collector, a stainless steel rotating cylinder was used. The electrospinning experiments were carried out with a distance of 8 cm between the nozzle and the collector. A 20 kV voltage was applied to the electrospinning solution to form a Taylor cone at the tip of the spinneret. The electrospun fibers were dried for 48 h at 25 °C, then treated for 4 h at 250 °C (heating rate 1 °C/min) and 4 h at 625 °C (heating rate 5 °C/min).

2.3 Scaffold Preparation

In the study to prepare the disc-shaped bioactive glass scaffolds, synthesized bioactive glass powders and the nanofibers were filled in the disc shape of alumina molds and the molds were put directly in a furnace operating at 690 °C for 1 h. At the end of one hour samples were immediately taken out of the furnace and cooled down to the room temperature before removing from the mold. Fabricated, glass scaffolds were utilized in cell culture and drug release experiments.

2.4 Characterizations

A scanning electron microscope (SEM, Zeiss, Gemini 500) was used to investigate the morphology of the fabricated bioactive glass powders and nanofibers. A particle size analyzer (Malvern, Mastersizer 3000, UK) was used to determine the particle size of the bioactive glass powders. Average fiber diameter was obtained from the SEM images of the samples by measuring the diameter of the approximately 40 fibers randomly. Phase analysis of the manufactured bioactive glass samples was made using an X-ray diffractometer (Malvern Panalytical,UK) using Cu Kα radiation at a scanning rate of 0.01°/min in the range of 10–90°.

Additionally, an optical microscope (Nikon Eclipse LV 100) was utilized to observe the morphology of the prepared particle and nanofiber-based bioactive glass disc-shaped scaffolds. The porosity of the glass scaffolds under investigation was obtained based on the Archimedes method which allowed the measurement of total and interconnected porosity. Measurements were performed using ethanol as the bouncy liquid. Total porosity was calculated based on Eq. (1) [27]:

$$P(\%) = \frac{(W_2 - W_1 - W_S)}{(W_1 - W_3)} x100 \quad (1)$$

where w_1 is considered the weight of the bottle filled with ethanol; w_2 represents the weight of the bottle filled with ethanol after immersion of the scaffold; w_3 is the weight of the bottle filled with ethanol after removal of the scaffold, and; ws is the weight of the dry weight of the scaffold.

2.4.1 In Vitro *Bioactivity*

In simulated body fluid (SBF) at 37 °C under static conditions, the ability of the produced bioactive glasses in the form of particles and nanofiber to deposit hydroxyapatite was investigated. SBF was prepared according to the methodology described by Kokubo et al. [28]. Bioactive glass samples were immersed in SBF with an initial pH of 7.4 (1 gr sample per 500 mL SBF) and stored in an incubator for 7, 14, and 30 days. Then, samples were removed from SBF, rinsed, and dried for at least 48 h at 60 °C before being characterized. SEM and FTIR-ATR Spectrometer (Thermo-Scientific, Nicolet IS20, USA) were used to assess the conversion to HA of the SBF-treated bioactive glass samples.

2.4.2 Cell Culture Studies

2.4.2.1 MTT Assay In the study, MTT (3-(4,5-dimethylthiazol-2-yl)-2,5-diphenyl-tetrazolium bromide) technique was used to examine the sample's cytotoxicity using osteoblastic MC3T3-E1 Subclone 4 cells (ATCC, CRL-2593 USA). Alpha-MEM with L-glutamine containing 10% FBS and 100 U/mL penicillin—100 mg/mL streptomycin was used to grow the osteoblastic MC3T3-E1 cells. Before cell culture studies, dry heat sterilization at 350 °C was applied to the scaffolds. Then scaffolds were submerged in anhydrous ethyl alcohol overnight and UV-sterilized for 2 h. In 24-well plates, 5.10^4 cells were seeded onto each scaffold in 100 µL of culture media. They were cultured for 72 h at 37 °C in a 5% CO_2 incubator. After that, MTT solution was added to each well, and the cells were cultured for another 4 h. The growth media was then withdrawn, and the produced formazan crystals were dissolved with dimethyl sulfoxide (DMSO, Sigma-Aldrich, Germany). A UV-spectrophotometer (Thermo-Scientific, Evolution 201, USA) was used to measure the amount of formazan at a wavelength of 570 nm.

2.4.2.2 Cell Morphology Morphology of the cells during cell culture studies was investigated using an inverted phase-contrast microscope (Olympus IX53, Japan). Additionally, the morphology of the cells seeded onto the scaffolds was analyzed using SEM. For this purpose, scaffolds

with attached cells were rinsed three times with PBS, fixed with 2.5% glutaraldehyde solution, and maintained in PBS at 4 °C overnight after 72 h of incubation. The scaffolds were then rinsed three times with PBS and dehydrated for 15 min in a graded series of ethyl alcohol solutions (gradually 50% to 100%) before being dried in hexamethyldisilazane (HMDS, Sigma Aldrich, Germany) for 10 min. Then samples were coated with gold/palladium and analyzed using SEM.

2.4.3 Drug Release Experiments

In the study, amoxicillin trihydrate ($C16H_{19}N_3O_5S{\cdot}3H_2O$, Sigma-Aldrich, Germany), one of the broad-spectrum antibiotics used in the treatment of osteomyelitis, which has a bactericidal effect against gram-positive and gram-negative microorganisms, was used as a drug model. As with other penicillin antibiotics, amoxicillin trihydrate has a bactericidal effect by inhibiting bacterial cell wall synthesis [29, 30].

For the drug loading studies, an automatic micropipette was utilized to transfer a drug solution (1 mg/mL) to the surface of the disc-shaped bioactive glass scaffolds. Drug-loaded scaffolds were dried for 24 h at room temperature. They were then immersed in a 5 mL phosphate buffer saline (PBS) solution with a pH of 7.4 as a starting point. A 2 ml sample was obtained from the release medium at defined time intervals for the release investigations, and the drug concentration was measured using a UV–Vis Spectrometer (Thermo-Scientific, Evolution 201, USA) @ 272 nm. After each measurement, 2 mL of fresh PBS was added to the release medium. The cumulative amoxicillin trihydrate release percentage from the scaffolds to the PBS medium was calculated using the drug's calibration curve. At room temperature, the experiments were conducted with at least three different measurements for each condition.

In the study, drug release kinetics was investigated using zero-order, first-order, and Higuchi kinetic models [31, 32]. The zero-order kinetic model is shown by Eq. (2):

$$C_t = C_0 + K_0 t \tag{2}$$

where C_t is the concentration of drug release in time t, C_0 is the initial concentration of the drug, and the K_0 is a zero-order constant. For zero-order kinetics, the release of a drug is only a function of time and the process takes place at a constant rate independent of the drug concentration [31].

The first-order kinetic model is represented by Eq. (3):

$$logQ_1 = logQ_0 + \frac{K_1 t}{2.303} \tag{3}$$

where Q_1 is the amount of drug released on time t, Q_0 is the initial amount of drug dissolved, K_1 is the first-order constant. Based on this model, the amount of drug released from a porous matrix is proportional to the amount of drug remaining in the matrix. As a result, the amount of active agents released decreases with time [31, 32].

On the other hand, the Higuchi model is shown by Eq. (4), where K_H is the release constant [31]:

$$Q = K_H \sqrt{t} \tag{4}$$

2.4.4 Statistical Analysis

The statistical analyses for the MTT test results were made with Graph Pad Prism 5. Results were analyzed by using one-way ANOVA. Values with $p \leq 0.05$ (*), $p \leq 0.01$ (**), were considered statistically significant.

3 Results and Discussion

3.1 Structural and Morphological Properties

SEM micrographs of the bare and XRD patterns of the rare-earth ion-containing 13–93 bioactive glasses in the form of sol–gel-derived particle and electrospun nanofiber are shown in Fig. 1. After size reduction, the median particle size of the bare bioactive glass powders was measured to be ~ 3.0 µm. The median particle size of the bioactive glasses containing rare-earth ions at different concentration was approximately the same. On the other hand, based on SEM micrographs, the average fiber diameter of 13–93 glass was determined to be 490 ± 35 nm. Similarly, the 5% Er^{3+} and 5% Tb^{3+}-doped bioactive glass samples had fiber diameters of 650 ± 180 nm and 290 ± 89 nm, respectively (Fig. 2).

XRD analysis results given in Fig. 1c and d demonstrated all of the bioactive glass samples prepared in the study have an amorphous structure. The introduction of the rare earth dopant even at the highest concentration did not cause crystallization in the glass structure. Figure 2 depicts the formation of continuous fibrous bare and the rare earth element doped glass network. The inclusion of the erbium and terbium (III) was not detrimental to the electrospinning process and nanofiber formation.

3.2 In Vitro *Bioactivity*

In the study, the HA formation ability of the studied glasses was investigated in SBF under static conditions. Figure 3, shows the FTIR spectra of the SBF-treated powders after 7 and 14 days of treatment. In the spectra, the band at 1032 cm^{-1} is corresponding to symmetric stretching

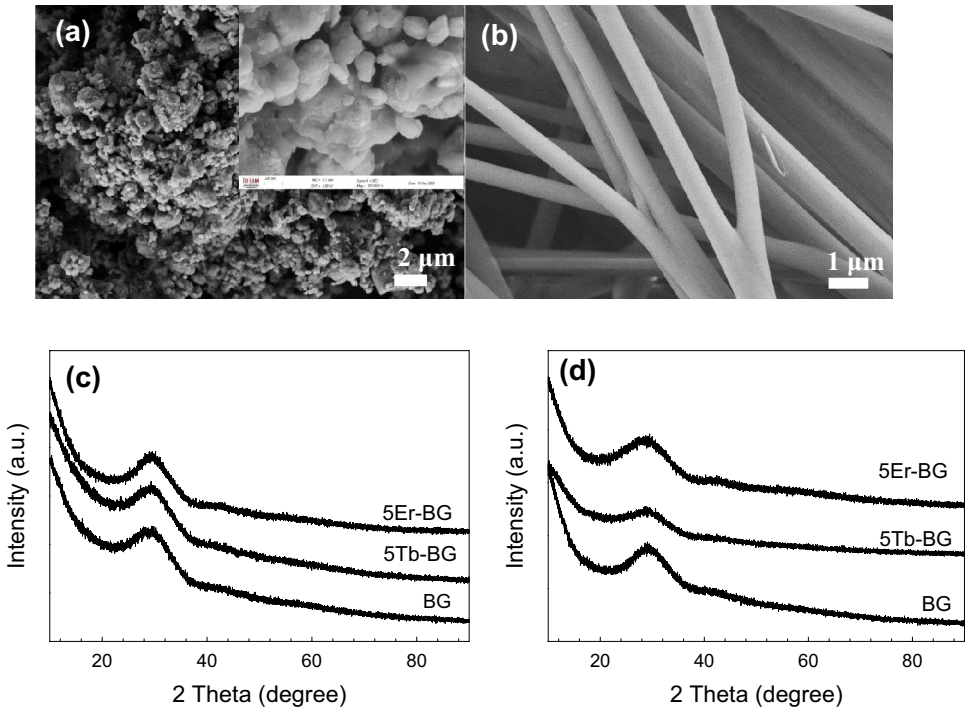

Fig. 1 SEM micrographs of the prepared pristine bioactive glass: **a** particles, **b** nanofibers; XRD patterns of the Er^{3+} and Tb^{3+}-containing bioactive glass: **c** particles, **d** nanofibers

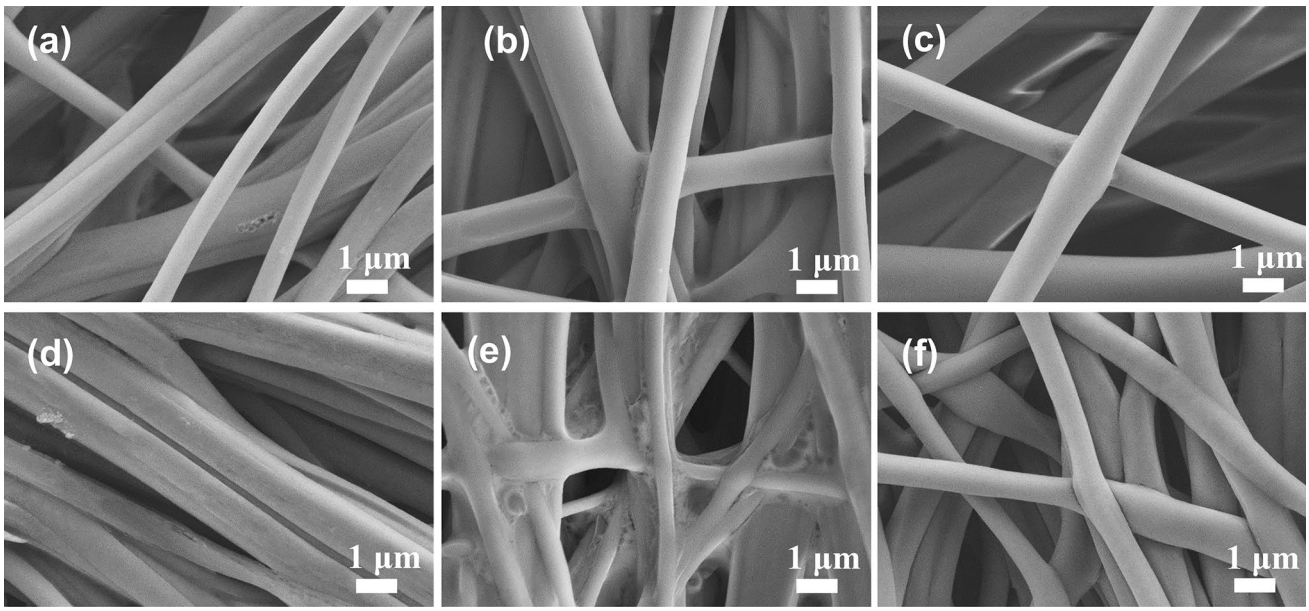

Fig. 2 SEM micrographs of the bioactive glass nanofibers prepared in the study: **a** 1%Er^{3+}, **b** 3%Er^{3+}, **c** 5%Er^{3+}, **d** 1%Tb^{3+}, **e** 3%Tb^{3+}, **f** 5%Tb^{3+}

vibration, v_3, of PO_4^{3-}. The peaks at 603 cm^{-1} and 564 cm^{-1} were assigned to the v_4 bending vibration of PO_4^{3-} [33]. Similarly, the sharp peak observed at ~ 460 cm^{-1} may be due to the ν_2 vibration of the PO_4^{3-} group [34]. Results revealed that starting from 7 days of treatment in SBF calcium phosphate-based material formation occurred on the surface of glass samples. Based on the FTIR analysis results in all of the studied bioactive glass powders treated in SBF for 14 days, HA formation (represented by the peaks at 603 cm^{-1} and 564 cm^{-1}) was obtained. The introduction of the rare-earth dopants to the glass structure did not cause a decrease in the bioactivity of the 13–93 glass. Similarly, SEM micrographs shown in Fig. 4 and Fig. 5, clearly verify the formation of a second phase material on the surface of the bioactive glass powders treated in SBF for 30 days. The morphology of the converted material, cauliflower-like

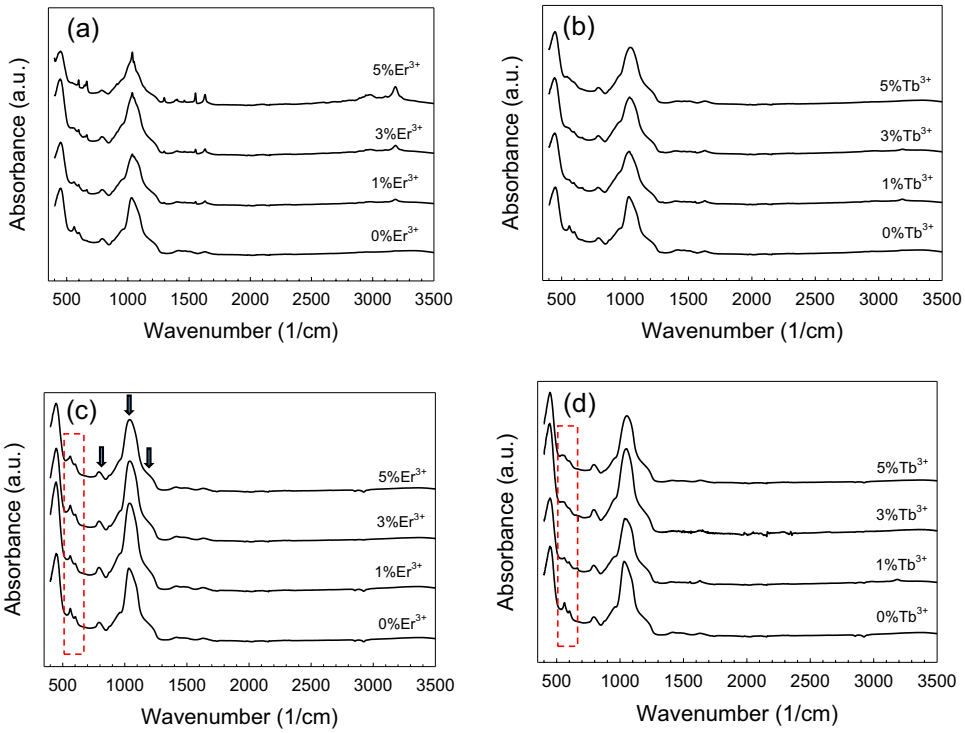

Fig. 3 FTIR spectra of the Er^{3+} and Tb^{3+}-containing bioactive glass powders treated in SBF for **a**, **b** 7 days; **c**, **d** 14 days

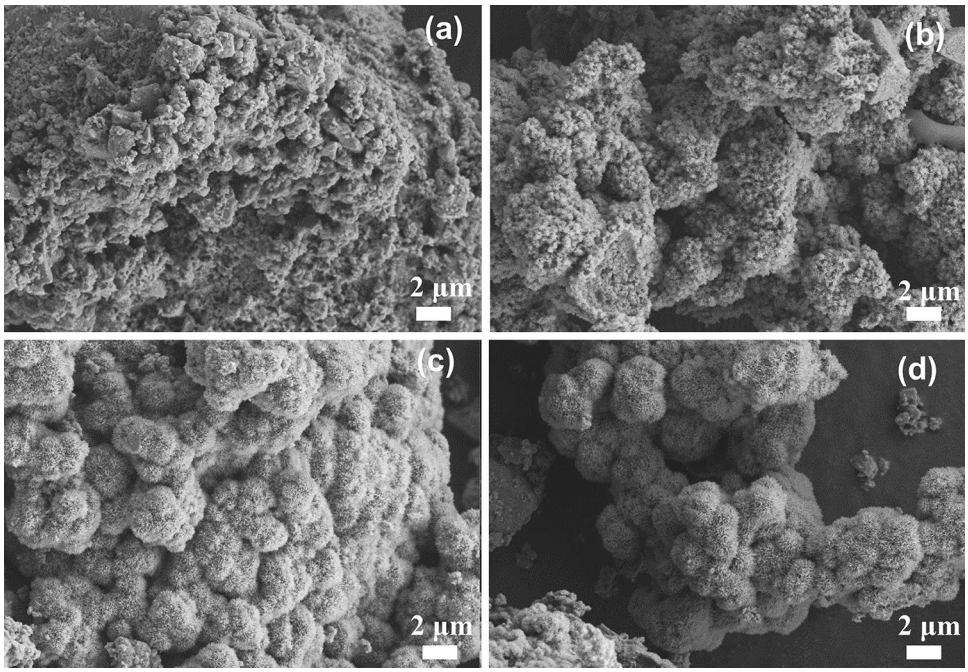

Fig. 4 SEM micrographs of the bioactive glass powders treated in SBF for 30 days: **a** bare, **b** 1%Er^{3+}, **c** 3%Er^{3+}, **d** 5%Er^{3+}

calcium phosphate agglomerates, confirm the HA deposition [35].

Based on the previous study of Alshemary et al.[36] in vitro bioactivity experiments performed for Er^{3+}-doped hydroxyapatite in SBF revealed the production of an apatite layer with a (Ca + Er)/P ratio in the range of 1.59–1.72. Similarly, Wang et al. [23] investigated the in vitro HA formation of sol–gel-derived Tb^{3+}-containing mesoporous bioactive glass nanospheres. Results indicated that the incorporation of Tb^{3+} ions in the glass nanospheres improved the hydroxyapatite formation ability.

The FTIR-ATR spectra of the synthesized bioactive glass nanofibers after treatment in SBF for 7 and 14 days are given in Fig. 6. Accordingly, calcium phosphate-based material

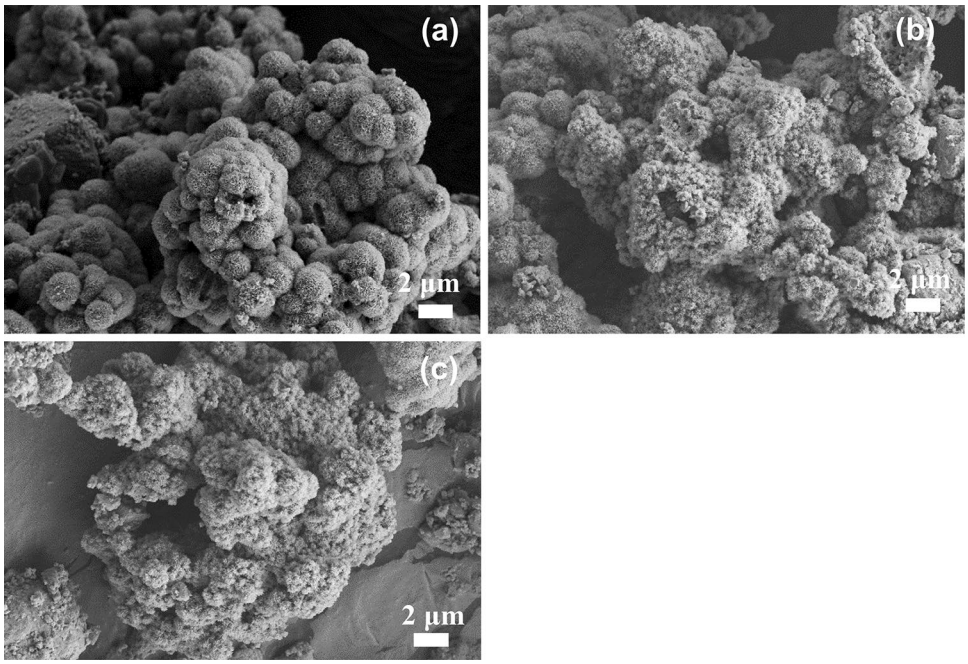

Fig. 5 SEM micrographs of the bioactive glass powders treated in SBF for 30 days: **a** 1%Tb^{3+}, **b** 3%Tb^{3+}, **c** 5%Tb^{3+}

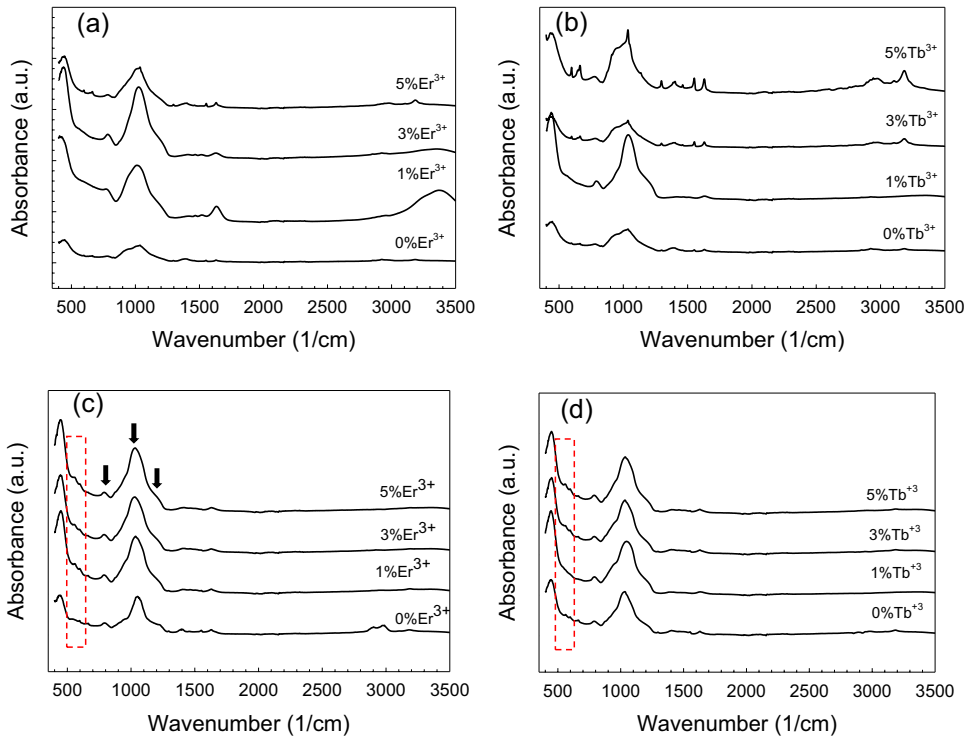

Fig. 6 FTIR spectra of the Er^{3+} and Tb^{3+}-containing electrospun bioactive glass nanofibers treated in SBF for **a**, **b** 7 days; **c**, **d** 14 days

formation was observed for all of the studied nanofibers after 14 days of immersion. However, the intensity of the band at ~ 1050 cm^{-1} was low compared to the results of the bioactive glass particle-based samples treated under the same conditions. After 7 days of immersion in SBF few samples, including the pristine 13–93 glass fibers, were converted to the calcium phosphate-based material. SEM micrographs of the bioactive glass nanofibers immersed in SBF for 30 days also support the FTIR analysis results (Fig. 7). Interestingly, although individual bioactive glass fibers have a high aspect ratio (that is, length/diameter) they gained lower bioactivity compared to the particle-based glass samples. Previously Li et al. [37] reported that by the use of the nanofibers the biocompatibility and bioactivity of materials can be improved.

The high aspect ratio, as well as the surface area of nanofibers, enable them to concentrate specified proteins on the surface to stimulate cell attachment and growth [37]. In the current study, the difference obtained in the bioactivity of the bioactive glass samples having spherical or fibrous morphology is presumably due to the difference in their surface area which directly influences their degradation rates in SBF. In bioactivity studies, sol-derived glass particles have been immersed in SBF after grinding which creates a higher total surface area however electrospun glass fibers were in the form of two-dimensional sheets when they were immersed in SBF.

3.3 Cytotoxicity Evaluation

In the study, cell culture experiments and drug release studies were performed using disc-shaped bioactive glass scaffolds prepared using synthesized glass particles and nanofibers. Figure 8 depicts the images of the prepared scaffolds from optical microscope analysis and their calculated porosity values based on the Archimedes method. Optical microscope images show the existence of a highly porous network and a rough surface in nanofiber-based bioactive glass scaffolds. On the other hand, the surface of the particle-based glass scaffolds was much smoother with smaller pores. The total porosity of the nanofiber-based glass scaffolds was calculated to be in the range of 55% to 65% whereas the porosities of the glass particle-based scaffolds were 15–25% under the same conditions.

The cytotoxicity of the prepared glass samples containing different concentrations of rare-earth dopants was examined by MTT assay using osteoblastic MC3T3-E1 cells. Figure 9 depicts the absorbance values representing the viability rates of the cells after incubation for 72 h. Accordingly, a decrease in cell viability was observed for the Er^{3+}-containing glass particle-based scaffolds starting from the 3 wt%. A further decrease was obtained in cell viability for the samples containing 5% Er^{3+}. On the other hand, any cytotoxicity was not observed for the glass nanofiber-based glass scaffolds containing erbium at the same concentrations. Similarly, terbium-containing glass scaffolds (both glass particle and nanofiber-based) did not cause any detrimental effect on cell viability at all concentrations. Since it has been known that the nanofibrous-based scaffolds or mats have higher biocompatibility compared to the particle-based systems due to their high surface area, it is not surprising to obtain a better cellular response in the case of Er^{3+}-containing nanofibrous-based glass scaffolds even at high dopant concentrations.

SEM micrographs of the MC3T3-E1 cells seeded (after 72 h) on to the particle and nanofiber-based bioactive glass scaffolds are shown in Figs. 10 and 11, respectively. Accordingly, in both particle- and the nanofibers-based bioactive glass samples cells attached and spread well onto the surface of the scaffolds. The morphology of the osteoblastic cells was flat, additionally the filopodia attached to the surface of the scaffold. The strong cell adherence may be due to the mechanical binding between the scaffold and cell surface and the filopodia.

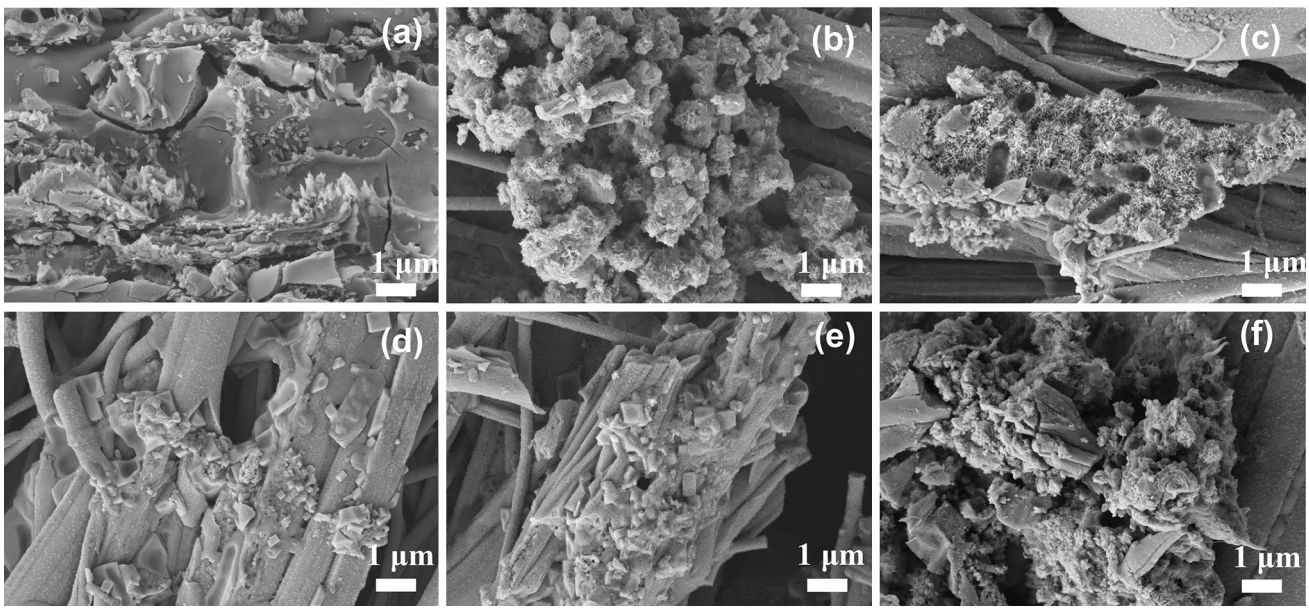

Fig. 7 SEM micrographs of the electrospun bioactive glass nanofibers treated in SBF for 30 days: **a** 1%Er^{3+}, **b** 3%Er^{3+}, **c** 5%Er^{3+}, **d** 1%Tb^{3+}, **e** 3%Tb^{3+}, **f** 5%Tb^{3+}

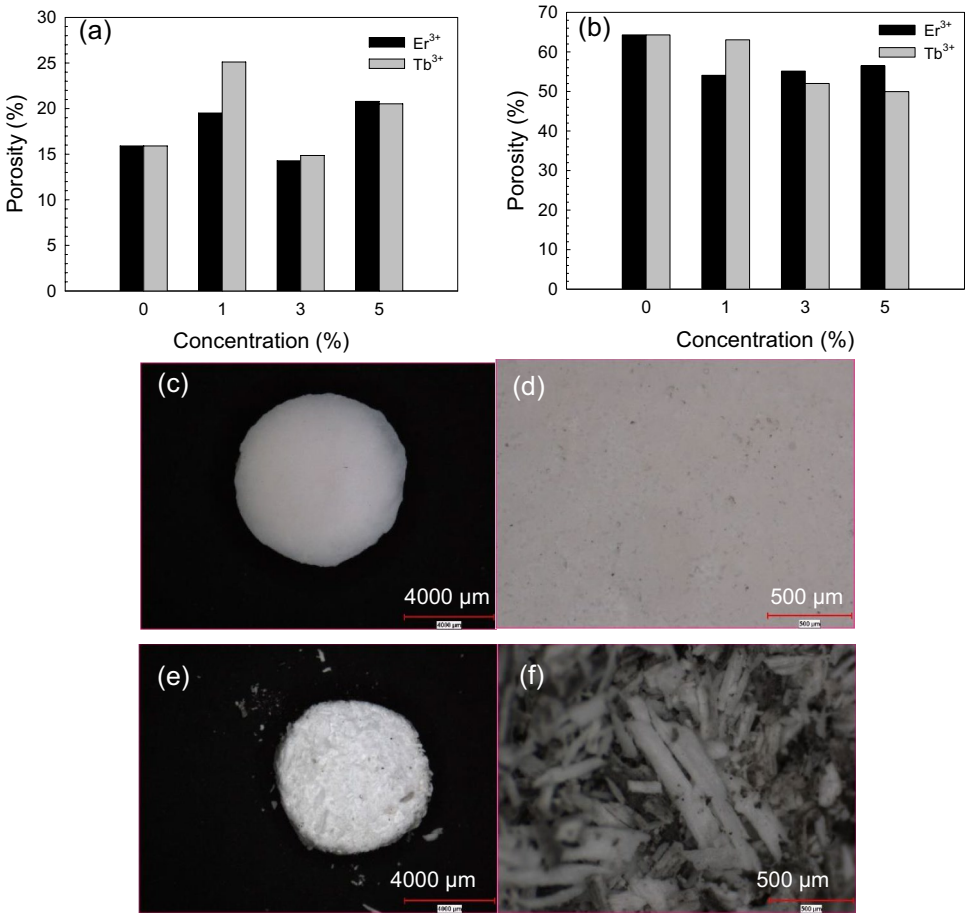

Fig. 8 Graphs showing the total porosity values of the bioactive glass: **a** particle-based, **b** nanofiber-based scaffolds; optical microscope images of the bare 13–93 glass **c**, **d** particle-based and **e**, **f** nanofiber-based scaffolds

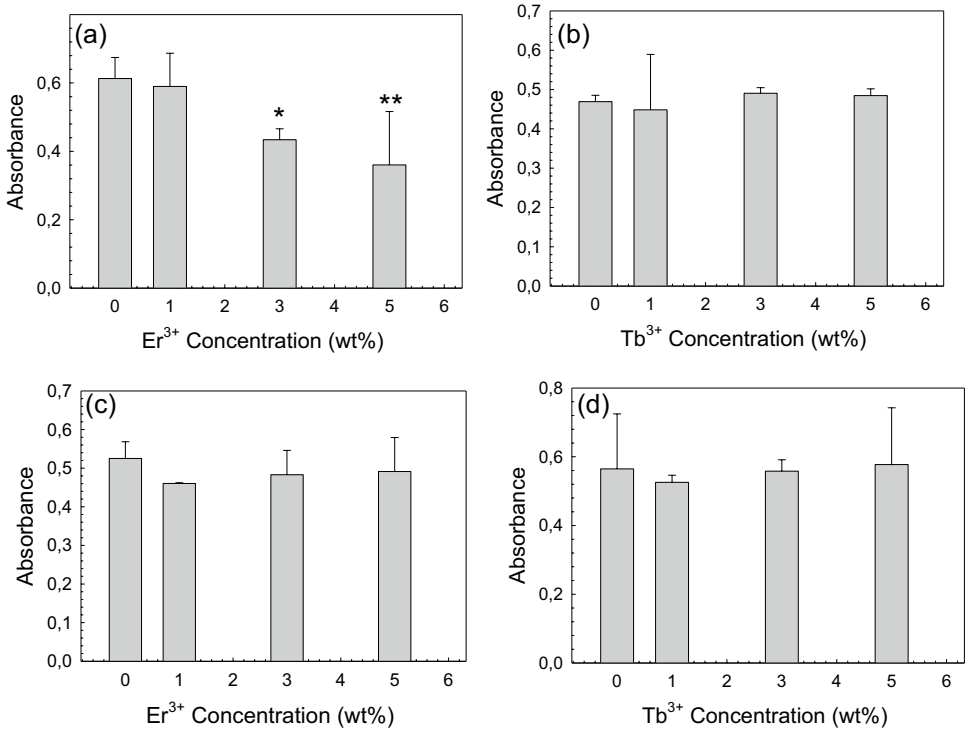

Fig. 9 Graphs showing the MTT assay results for Er^{3+} and Tb^{3+}-containing bioactive glass scaffolds fabricated using **a**, **b** particles; **c**, **d** nanofibers

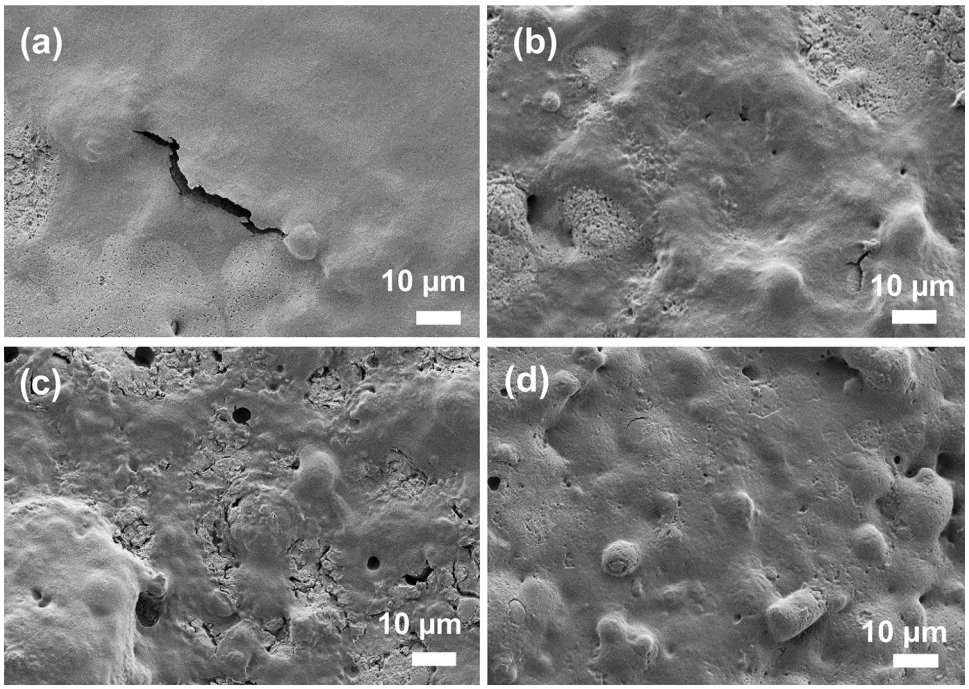

Fig. 10 SEM micrographs of the MC3T3-E1 cells seeded onto the **a** bare, **b** 1%Er^{3+}, **c** 3%Er^{3+}, **d** 5%Er^{3+}-containing glass particle-based scaffolds after 72 h incubation

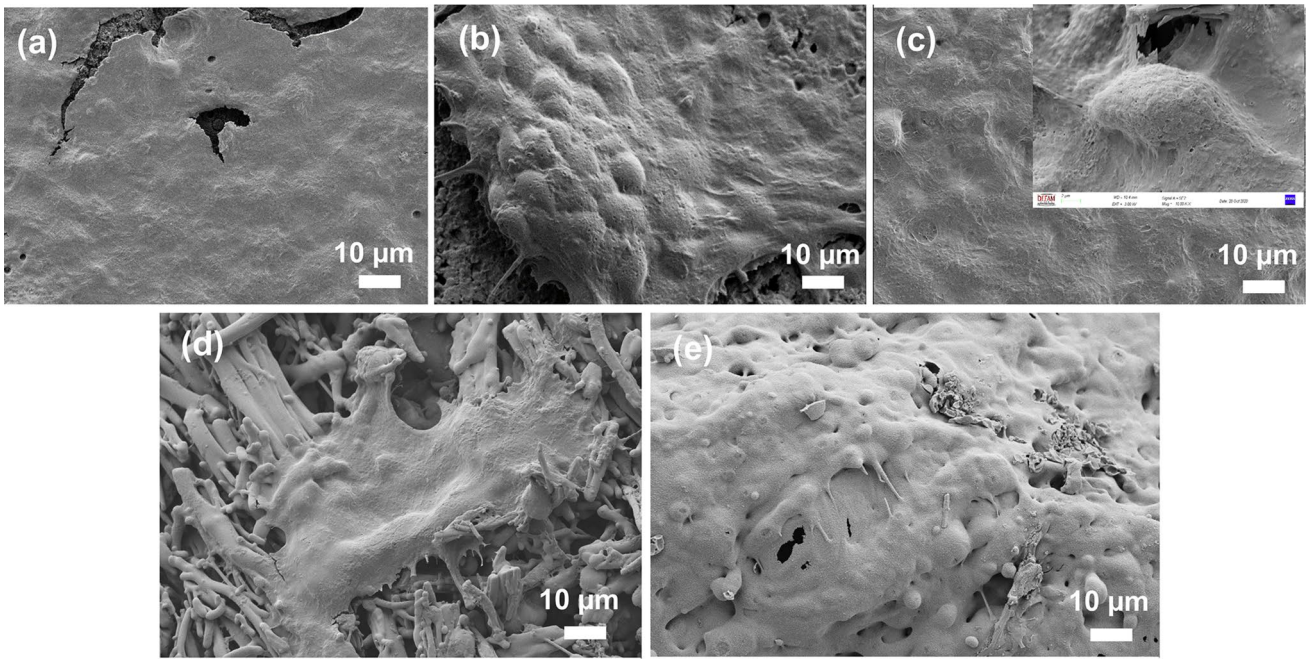

Fig. 11 SEM micrographs of the MC3T3-E1 cells seeded onto the **a** 1%Tb^{3+}, **b** 3%Tb^{3+}, **c** 5%Tb^{3+}-containing glass particle, **d** 5%Er^{3+} and **e** 5%Tb^{3+}-containing glass nanofiber-based scaffolds after 72 h incubation

Optical microscope images of the MC3T3-E1 cells cultured for 72 h in the presence of fabricated glass particle and the nanofiber-based scaffolds are given in Figs. 12 and 13, respectively. A significant difference was not observed in the cell morphology depending on the rare-earth element type. However, cells cultured in the presence of Er^{3+} and Tb^{3+}-containing glass scaffolds spread better, achieved higher confluency, and started to form a monolayer in culture dishes compared to the cells culture with pristine glass scaffolds. In general, MC3T3-E1 cells exhibited a partially rounded form and also displayed a polygonal morphology with extended cytoplasm on the 3rd day of culture with the glass scaffolds.

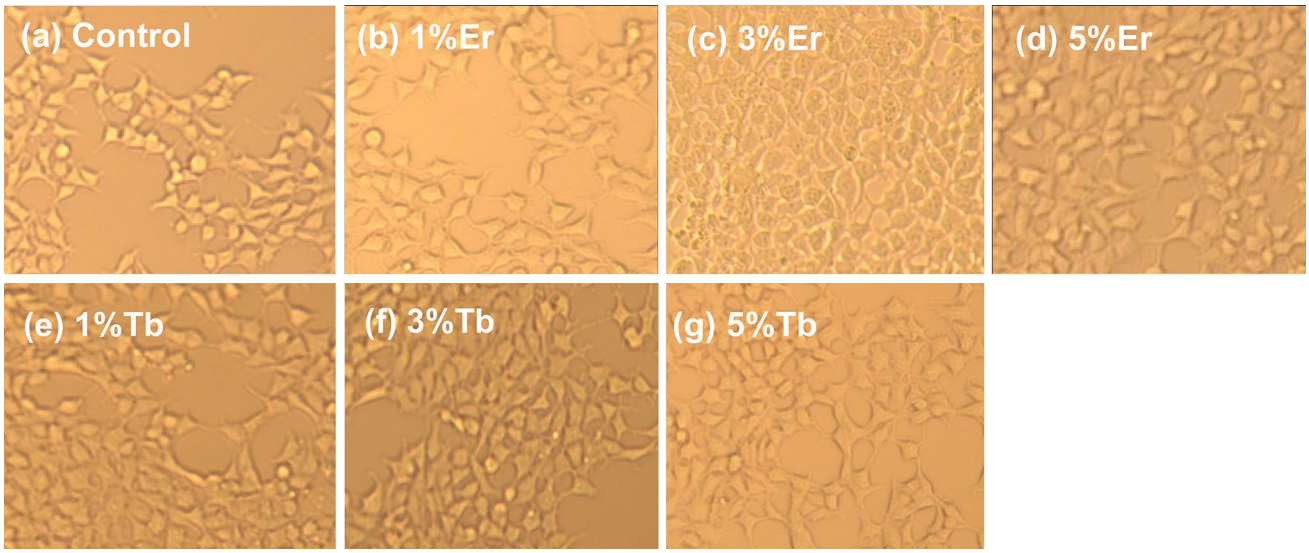

Fig. 12 Optical microscope images of the MC3T3-E1 cells cultured with the **a** bare, **b** 1%Er^{3+}, **c** 3%Er^{3+}, **d** 5%Er^{3+}, **e** 1%Tb^{3+}, **f** 3%Tb^{3+}, **g** 5%Tb^{3+}-containing glass particle-based scaffolds for 72. Magnification: 100x

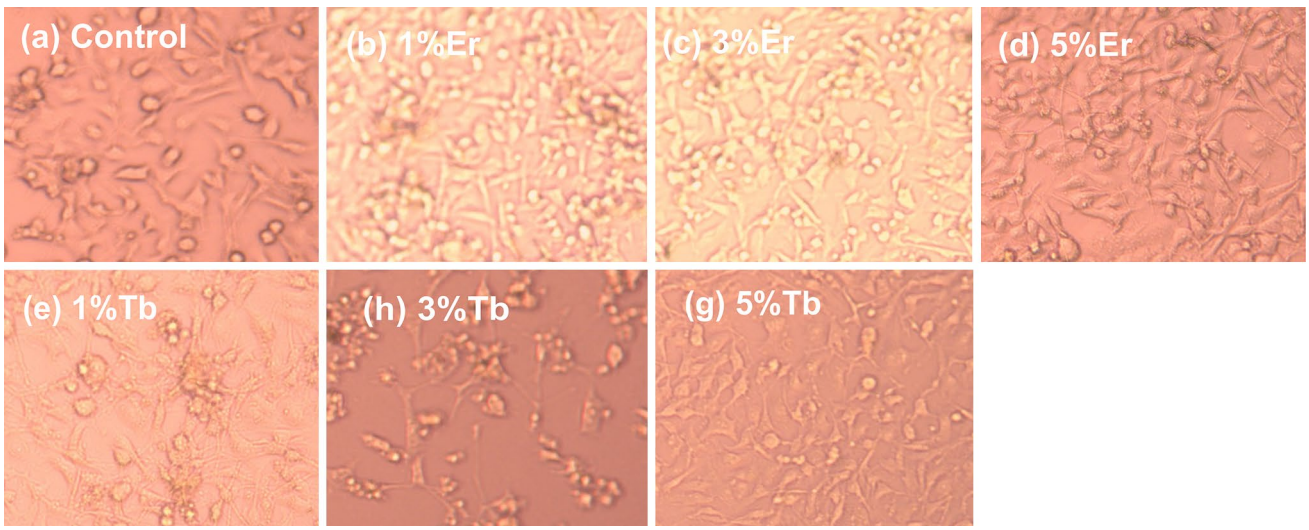

Fig. 13 Optical microscope images of the MC3T3-E1 cells cultured with the **a** bare, **b** 1%Er^{3+}, **c** 3%Er^{3+}, **d** 5%Er^{3+}, **e** 1%Tb^{3+}, **f** 3%Tb^{3+}, **g** 5%Tb^{3+}-containing glass nanofiber-based scaffolds for 72 h. Magnification: ×100

There are very limited studies in the literature regarding the biological properties of erbium-containing biomaterials. Wu et al. [38] studied the piezoelectric and biological characteristics of Er^{3+}-doped barium titanate/hydroxyapatite (BT/HA) composites. The addition of Er^{3+} to BT/HA promoted osteoblast proliferation more than the lack of erbium ions [38]. Low Er^{3+} concentrations have been shown to stimulate cell protein synthesis and increase mitochondrial succinate dehydrogenase activity, both of which increase cell proliferation. Er^{3+} can not only occupy the Ca^{2+} site but also substitute bound calcium to enhance intracellular Ca^{2+} levels because Er^{3+} and Ca^{2+} share many properties and structures. It is well understood that during cell proliferation, an increase in Ca^{2+} content in the cytosol is required. As a result, Er^{3+} can help cells proliferate by allowing extracellular Ca^{2+} to enter the cell [38, 39].

Wei et al. [21] performed experiments on the response of osteoblastic MC3T3-E1 cells on terbium-doped HA nanorods at different concentrations namely 25, 50, and 100 µg/mL. Based on the cell viability experiments, the optical density (representing the number of living cells) increased with the increase in incubation time, indicating that terbium-doped HA had no significant cell toxicity at given concentrations. This result, suggests the high

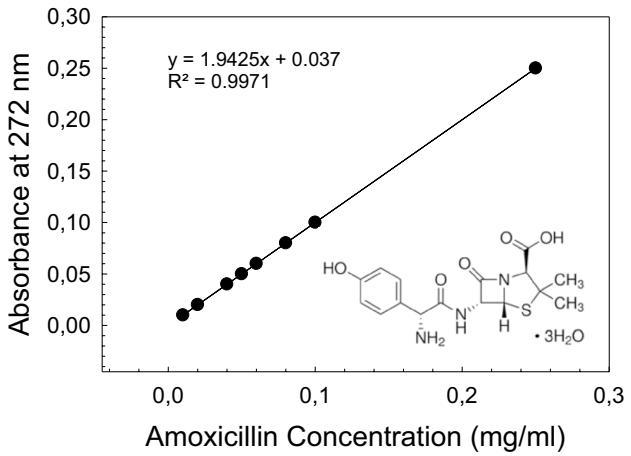

Fig. 14 Standard calibration curve obtained for the amoxicillin solutions and the chemical structure of the drug molecule

biocompatibility of terbium-containing biomaterials in intracellular cytoplasm.

3.4 Drug Release Behavior

In the current study, amoxicillin was chosen as the drug model to perform drug release experiments in PBS up to 220 h. The amoxicillin concentration was calculated from a standard calibration curve that obeys the Beer-Lambert law. For this purpose, a series of amoxicillin solutions in PBS with known concentrations were prepared and the optical density was recorded by a UV-spectrometer. Figure 14 shows the obtained calibration curve for the drug solution and the chemical structure of the amoxicillin trihydrate.

Figure 15 demonstrates the cumulative drug release percentages from bare and rare-earth element-containing particle and the nanofiber-based bioactive glass scaffolds as a function of time. Accordingly, the drug release amount from the particle-based glass scaffolds containing Er^{3+} was in the range of 33.5% to 38% in the first 24 h. At the end of 220 h, release amounts reached 92.5% to 96.2%. Similar drug release percentages were obtained for the Tb^{3+}-containing glass particle-based scaffolds for the first 24 h and the 220 h. On the other hand, after 220 h cumulative drug release percentages from the Er^{3+} or Tb^{3+} containing glass fiber-based scaffolds were in the range of 79% to 85%. In general, a decrease in cumulative drug release was observed by the increase in rare-earth ion concentration. Results also revealed that initially a burst release behavior (about 20% in the first 10 h) was followed by a sustained drug release behavior from all of the bioactive glass scaffolds tested in the study. It has been shown that about 50% of the drug remained in the scaffolds after 48 h and this may be beneficial for the inhibition of the bacterial growth for longer times. Results indicated that the sustained drug release behavior observed in the study may be suitable for the treatment of bone infections. On the other hand, the burst release behavior observed in the first period may be useful for the first days of implantation in a bone defect, when there is a high risk of inflammatory response and infection.

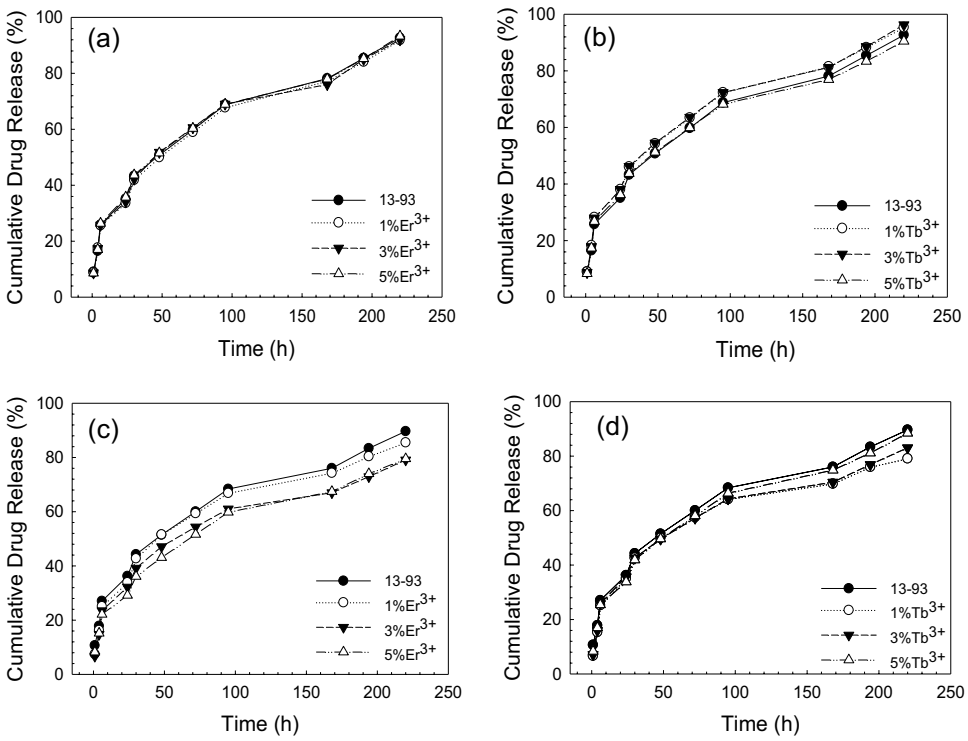

Fig. 15 Graphs showing the cumulative drug release percentage from Er^{3+} and Tb^{3+}-containing glass **a**, **b** particle-based; **c**, **d** nanofiber-based scaffolds as a function of time

In the study, observed burst release behavior may be attributed to the physical adsorption of the drug molecules and the glass surface. It is also important to note that, due to the presence of hydroxide (OH) groups, bioactive glasses gain a net negative surface charge [40]. This may be considered as difficulty in loading negatively charged amoxicillin to the glass surface. Meanwhile, amoxicillin is a water-soluble drug, and synthesized bioactive glasses have high hydrophilicity therefore the drug solution can easily reside in the free space of pores of fabricated glass scaffolds, which may increase the drug loading. Additionally, amoxicillin molecules contain hydroxyl groups (–OH) that may interact with silanols (Si–OH) and the P-OH groups on the surface of the bioactive glass samples through hydrogen bonding.

Previously, Bakhsheshi-Rad et al. [41] investigated the fabrication of bredigite–amoxicillin scaffolds for bone tissue engineering. Results revealed an initial burst release of amoxicillin (20%) in the first 8 h followed by a sustained release behavior up to 80 h. Similarly, Zheng et al. [42] reported the preparation of amoxicillin-loaded hydroxyapatite/poly(lactic-co-glycolic acid) nanofibers. Results showed that the drug was loaded into the related system by physical adsorption and the composite nanofibers showed a sustained release profile. Tabia et al. [43] studied the amoxicillin release from the Mg-doped mesoporous bioactive glass nanoparticles. An increase was obtained in the cumulative drug release as the Mg concentration was increased. Additionally, all of the release profiles followed first-order release kinetics which is characteristic of a diffusion process. Amudha et al. [44] analyzed the amoxicillin release of the mesoporous bioactive glass samples containing strontium ions. In the beginning, the drug release profile of bare and 1%Sr-containing samples showed burst release. On the other hand, bioactive glass samples containing higher concentrations of strontium demonstrated sustained drug release (58% and 75%) after 720 h due to their high surface area.

3.5 Drug Release Kinetics

Mathematical models are useful for designing pharmaceutical formulations and evaluating drug release mechanisms in vitro and in vivo. They enable the assessment of some critical physical characteristics (such as the drug diffusion coefficient) as well as model fitting using experimental release data. Mathematical analysis of drug release kinetics adds value by guaranteeing optimal formulation design and understanding of release mechanisms through experimental verification. Therefore, the release process an be understood through a precise combination of experimental observations and models that allow for the acquisition of the underlying physics [31, 45].

Tables 2 and 3 show the zero-order, first-order release kinetics and Higuchi model parameters (kinetic constant, k, and coefficient of determination, R^2) obtained from the release experiments. In the study, all the release profiles followed the Higuchi Model ($Q = K_H \cdot t^{1/2}$, where Q is the

Table 2 Kinetic model parameters (kinetic constant, k and coefficient of determination, R^2) obtained by applying different mathematical models on amoxicillin release profile of particle-based bioactive glass samples

Sample	Zero-order		First-order		Higuchi model	
	R^2	K_0	R^2	K_1	R^2	K_H
BG	0.8869	0.6463	0.9641	0.0112	0.9867	6.8156
1Er-BG	0.8901	0.6342	0.9646	0.0109	0.9858	6.6729
3Er-BG	0.8928	0.6528	0.9678	0.0114	0.9871	6.8627
5Er-BG	0.8812	0.6486	0.9616	0.0113	0.9854	6.8575
1 Tb-BG	0.8759	0.6788	0.9640	0.0124	0.9839	7.1927
3 Tb-BG	0.8765	0.6823	0.9644	0.0124	0.9845	7.2291
5 Tb-BG	0.8732	0.6399	0.9564	0.1110	0.9832	6.7889

Table 3 Kinetic model parameters (kinetic constant, k and coefficient of determination, R^2) obtained by applying different mathematical models on amoxicillin release profile of nanofiber-based bioactive glass samples

Sample	Zero-order		First-order		Higuchi model	
	R^2	K_0	R^2	K_1	R^2	K_H
BG	0.8735	0.6924	0.9566	0.0110	0.9831	6.708
1Er-BG	0.8803	0.6415	0.9573	0.0109	0.9851	6.785
3Er-BG	0.8739	0.5844	0.9453	0.0093	0.9841	6.200
5Er-BG	0.8994	0.5569	0.9600	0.0087	0.9871	5.834
1 Tb-BG	0.8612	0.6157	0.9415	0.0101	0.9803	6.567
3 Tb-BG	0.8587	0.6098	0.9408	0.0101	0.9794	6.512
5 Tb-BG	0.8829	0.6236	0.9589	0.0105	0.9851	6.589

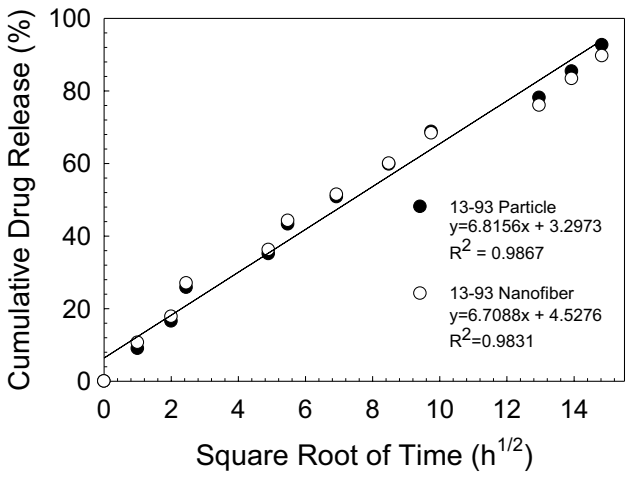

Fig. 16 Graph showing the application of Higuchi model on the drug release profiles of bare 13–93 bioactive glass particle and fiber-based scaffolds

amount of drug released at time t and k_h is the dissolution constant) [46, 47]. To analyze the release kinetics a straight-line was fitted through the data using the linear regression approach. The slope of the line represents the release rate constant, K_H. The quality of fit and how well the straight-line fits the real dissolution data are revealed by R^2. A high R^2 value close to unity suggested a good match to the Higuchi square root of time model, demonstrating that it could be utilized to characterize the drug release mechanism of bioactive glass scaffolds under investigation as diffusion-controlled [48]. According to the model parameters given in Tables 2 and 3, the presence of rare-earth ions, as well as the bioactive glass morphology, have some influence on the drug release rates. Higuchi release constant values of the glass particle-based samples are higher than the glass nanofiber-based counterparts.

Figure 16 shows the application of the Higuchi square root of time model to drug release profiles in bare 13–93 glass samples as an example. Both profiles matched the model well, as evidenced by strong coefficients of determination (R^2) calculated using linear regression analysis of sample dissolution data. A previous study by El-Kady et al. [49] has reported the release kinetics of another antibiotic, ciprofloxacin, from bioactive glass nanopowders. Similarly, the drug release profiles of all samples studied using Higuchi and Baker-Lonsdale models verified that the drug was released by a controlled diffusion means. Similarly, in a recent study [50], the release profiles of the vancomycin from bioactive glass-containing chitosan-based scaffolds have been expressed by the Higuchi model indicating that the release was mainly a diffusion-controlled mechanism.

To summarize, findings of the current study indicated that the fabricated Er^{3+} and Tb^{3+}-doped bioactive glasses can sustain the release of amoxicillin through a diffusion-based mechanism which may be an advantage in preventing bone infections, therefore, they have high potential to be used in bone tissue engineering applications. However, it is necessary to conduct some in vivo studies to confirm the effectiveness of those bioactive glasses under investigation.

4 Conclusions

Erbium and terbium (III)-containing 13–93 bioactive glasses were prepared in the form of particles and electrospun nanofibers. All of the glass samples studied have an amorphous structure after calcination performed at 625 °C. In vitro bioactivity experiments which were performed in SBF showed that synthesized bioactive glass samples have the ability to form HA on their surface after immersion in SBF. Particle-based glass samples converted to HA at a faster rate compared to the nanofiber-based glass samples. Cell viability experiments performed by MTT assay showed that Er^{3+} and Tb^{3+}-containing nanofiber-based glass samples were not cytotoxic to MC3T3-E1 cells at any dopant concentration however Er^{3+} doped particle-based samples caused a decrease in cell viability at high concentrations. Amoxicillin-loaded bioactive glass scaffolds showed burst release in the first period due to the sudden release of the drug molecules adhering to the surface glass. However, about 50% of the drug remained in the scaffolds after 48 h and this may be beneficial for the inhibition of the bacterial growth for longer times. Overall results indicated that the bioactive glass samples prepared in the study in the form of particle and nanofibers have high bioactivity in SBF and are biocompatible with osteoblastic MC3T3-E1 cells up to 72 h. Additionally, the sustained antibiotic release behavior observed in the study may be suitable for the treatment of bone infections. It was concluded that Er^{3+} and Tb^{3+}-containing bioactive glasses prepared in the study have the potential for bone regeneration, drug delivery, and bio-imaging applications.

Acknowledgements The authors acknowledge the financial support provided by the Scientific and Technological Research Council of Turkey (TÜBİTAK, Grant No.: 119M934).

Data Availability Any data that support the findings of this study are included within the article.

Declarations

Conflict of Interest The authors declare no conflict of interest regarding the publication of this paper.

References

1. L.L. Hench, Bioceramics. J. Am. Ceram. Soc. **81**(7), 1705–1728 (1998). https://doi.org/10.1111/j.1151-2916.1998.tb02540.x
2. L.L. Hench, Chronology of bioactive glass development and clinical applications. New J. Glass Ceram. **3**, 67–73 (2013)
3. M.N. Rahaman, D.E. Day, B. Sonny Bal, Q. Fu, S.B. Jung, L.F. Bonewald, A.P. Tomsia, Bioactive glass in tissue engineering. Acta Biomater. **7**(6), 2355–2373 (2011). https://doi.org/10.1016/j.actbio.2011.03.016
4. F. Baino, G. Novajra, V. Miguez-Pacheco et al., Bioactive glasses: special applications outside the skeletal system. J. Non-Cryst. Solids **243**, 15–30 (2016)
5. A. Polini, H. Bai, A.P. Tomsia, Dental applications of nanostructured bioactive glass and its composites. Wiley Interdiscip. Rev. Nanomed. Nanobiotechnol. **5**(4), 399–410 (2013)
6. J. Will, L.-C. Gerhardt, A.R. Boccaccini, Bioactive glass-based scaffolds for bone tissue engineering. Adv. Biochem. Eng. Biotechnol. (2011). https://doi.org/10.1007/10_2011_106
7. V. Mourino, J.P. Cattalini, A.R. Boccaccini, Metallic ions as therapeutic agents in tissue engineering scaffolds: an overview of their biological applications and strategies for new developments. J. R. Soc. Interface **9**(68), 401–419 (2012)
8. J.R. Jones et al., Controlling ion release from bioactive glass foam scaffolds with antibacterial properties. J. Mater. Sci. Mater. Med. **17**(11), 989–996 (2006)
9. I.A. Neacsu, A.E. Stoica, B.S. Vasile, E. Andronescu, Luminescent hydroxyapatite doped with rare earth elements for biomedical applications. Nanomaterials **9**(2), 239 (2019). https://doi.org/10.3390/nano9020239
10. Y. Fan, P. Yang, S. Huang, J. Jiang, H. Lian, J. Lin, Luminescent and mesoporous europium-doped bioactive glasses (MBG) as a drug carrier. J. Phys. Chem. C **113**(18), 7826–7830 (2009)
11. A. Baranowska, J.R. Dąbrowski, M. Kochanowicz, J. Dorosz, Effect of biodegradation on spectroscopic properties of Sm^{3+} doped 45S5 bioglass. In *Photonics Applications in Astronomy, Communications, Industry, and High-Energy Physics Experiments 2018*, Vol. 10808. (International Society for Optics and Photonics, 2018), p. 1080833. https://doi.org/10.1117/12.2500274
12. D.Y. Zhu, B. Lu, J.H. Yin, Q.F. Ke, H. Xu, C.Q. Zhang, Y.P. Guo, Y.S. Gao, Gadolinium-doped bioglass scaffolds promote osteogenic differentiation of hBMSC via the Akt/GSK3β pathway and facilitate bone repair in vivo. Int. J. Nanomed. **14**, 1085 (2019)
13. Y. Xue, Y. Du, J. Yan, Z. Liu, P.X. Ma, X. Chen, B. Lei, Monodisperse photoluminescent and highly biocompatible bioactive glass nanoparticles for controlled drug delivery and cell imaging. J. Mater. Chem. B **3**(18), 3831–3833 (2015)
14. T. Zambanini, R. Borges, P.C. Faria, G.P. Delpino, I.S. Pereira, M.M. Marques, J. Marchi, Dissolution, bioactivity behavior, and cytotoxicity of rare earth-containing bioactive glasses (RE= Gd, Yb). Int. J. Appl. Ceram. Technol. **16**(5), 2028–2039 (2019)
15. S. Zaichick et al., Accumulation of rare earth elements in human bone within the lifespan. Metallomics **3**(2), 186–194 (2011)
16. J. Diaci, B. Gaspirc, Comparison of Er: YAG and Er, Cr: YSGG lasers used in dentistry. J. Laser Health Acad. **1**(1), 1–3 (2012)
17. Q. Li, M. Xing, Z. Chen, X. Wang, C. Zhao, J. Qiu et al., Er^{3+} /Yb^{3+} co-doped bioactive glasses with up-conversion luminescence prepared by containerless processing. Ceram. Int. **42**(11), 13168–13175 (2016)
18. V.-H. Pham, H.N. Van, P.D. Tam, H.N.T. Ha, A novel 1540 nm light emission from erbium doped hydroxyapatite/-tricalcium phosphate through co-precipitation method. Mater. Lett. **167**, 145–147 (2016)
19. B.J. Allen, N. Blagojevic, Alpha- and beta-emitting radiolanthanides in targeted cancer therapy: the potential role of terbium-149. Nucl. Med. Commun. **17**, 40–47 (1996)
20. L. Li, Y. Liu, J. Tao, M. Zhang, H. Pan, X. Xu, R. Tang, Surface modification of hydroxyapatite nanocrystallite by a small amount of terbium provides a biocompatible fluorescent probe. J. Phys. Chem. C **112**, 12219–12224 (2008)
21. Y. Wei, Y. He, X. Li, H. Chen, X. Deng, Cellular uptake and delivery-dependent effects of Tb3+-doped hydroxyapatite nanorods. Molecules **22**, 1043 (2017)
22. A.V. Paduraru, O. Oprea, A.M. Musuc, B.S. Vasile, F. Iordache, E. Andronescu, Influence of terbium ions and their concentration on the photoluminescence properties of hydroxyapatite for biomedical applications. Nanomaterials. **11**(9), 2442 (2021)
23. X. Wang, Y. Zhang, C. Lin, W. Zhong, Sol-gel derived terbium-containing mesoporous bioactive glasses nanospheres: in vitro hydroxyapatite formation and drug delivery. Colloids Surf. B **160**, 406–415 (2017)
24. A.M. Deliormanlı, B. Rahman, S. Oguzlar, K. Ertekin., Structural and luminescent properties of Er^{3+} and Tb^{3+}-doped sol–gel-based bioactive glass powders and electrospun nanofibers. J. Mater. Sci. **56**, 14487–14504 (2021). https://doi.org/10.1007/s10853-021-06203-7
25. A.M. Deliormanli, S.A. Issa, M.S. Al-Buriahi, B. Rahman, H.M. Zakaly, H.O. Tekin, Erbium (III)-and Terbium (III)-containing silicate-based bioactive glass powders: physical, structural and nuclear radiation shielding characteristics. Appl. Phys. A **127**(6), 1–8 (2021)
26. A.M. Deliormanlı, Preparation, in vitro mineralization and osteoblast cell response of electrospun 13–93 bioactive glass nanofibers. Mater. Sci. Eng. C **53**, 262–271 (2015). https://doi.org/10.1016/j.msec.2015.04.037
27. S.Z. Jalise, N. Baheiraei, F. Bagheri, The effects of strontium incorporation on a novel gelatin/bioactive glass bone graft: In vitro and in vivo characterization. Ceram. Int. **44**(12), 14217–14227 (2018)
28. T. Kokubo, H. Takadama, How useful is SBF in predicting in vivo bone bioactivity? Biomaterials **27**, 2907–2915 (2006). https://doi.org/10.1016/j.biomaterials.2006.01.017
29. A. Bonifaz, A. Tirado-Sánchez, L. Calderón, G. Montes de Oca, P. Torres-Camacho, R.M. Ponce, Treatment of cutaneous actinomycosis with amoxicillin/clavulanic acid. J. Dermatol. Treat. **28**(1), 59–64 (2017)
30. Weber DJ, Tolkoff-Rubin NE, Rubin RH. Amoxicillin and potassium clavulanate: an antibiotic combination. Mechanism of action, pharmacokinetics, antimicrobial spectrum, clinical efficacy and adverse effects. Pharmacotherapy. 4(3):122–36 (1984). https://doi.org/10.1002/j.1875-9114.1984.tb03333.x
31. Bruschi ML, Mathematical models of drug release, Strategies to Modify the Drug Release from Pharmaceutical Systems. Woodhead Publishing (2015). 63–86. ISBN 9780081000922. https://doi.org/10.1016/B978-0-08-100092-2.00005-9
32. T. Nandi, M.A. Rahman, N. Jahan, R.S. Islam, O.F. Pavel, Determination of in-vitro release kinetics of metformin hydrochloride from six brands of metformin hydrochloride tablets available in bangladesh using water media: a UV spectroscopic analysis. Spec. J. Med. Res. Health Sci. **2**(2), 8–16 (2017)
33. Q. Yao, Z. Song, J. Lia, L. Zhang, Micromorphology, mechanical, crystallization and permeability properties analysis of HA/PBAT/PLA (HA, hydroxyapatite; PBAT, poly(butylene adipate-co-butylene terephthalate); PLA, polylactide) degradability packaging films. Polym. Int. (2019). https://doi.org/10.1002/pi.5953
34. L. Berzina-Cimdina, N. Borodajenko, Research of calcium phosphates using fourier transform. Infrared Spectrosc. Infrared Spectrosc., Prof. Theophanides Theophile (Ed.), ISBN: 978-953-51-0537-4, InTech (2012)

35. F. Baino, Copper-doped ordered mesoporous bioactive glass: a promising multifunctional platform for bone tissue engineering. Bioengineering **7**(2), 45 (2020). https://doi.org/10.3390/bioengineering7020045
36. A.Z. Alshemary, M. Akram, Y.-F. Goh, M.R. Abdul Kadir, A. Abdolahi, R. Hussain, Structural characterization, optical properties and in vitro bioactivity of mesoporous erbium-doped hydroxyapatite. J. Alloys Compd. **645**, 478–486 (2015)
37. X. Li, R. Cui, W. Liu, L. Sun, B. Yu, Y. Fan, Q. Feng, F. Cui, F. Watari, The use of nanoscaled fibers or tubes to improve biocompatibility and bioactivity of biomedical materials. J. Nanomater. **2013**, Article ID 728130 (2013). https://doi.org/10.1155/2013/728130
38. C. Wu, Y. Tang, K. Zhao, M. Jiao, Z. Wu, Erbium-doped barium titanate/hydroxyapatite composites with enhanced piezoelectric and biological properties. Micro Nano Lett. **15**(7), 421–424 (2020)
39. J. Zhang, X. Li, S. Xu et al., Effects of rare earth ions on proliferation, differentiation and functional expression of osteoblasts cultured in vitro. Prog. Nat. Sci. **14**(4), 404–409 (2004).
40. A. Doostmohammadi, A. Monshi, R. Salehi et al., Bioactive glass nanoparticles with negative zeta potential. Ceram. Int. **37**, 2311–2316 (2011)
41. H. Bakhsheshi-Rad, E. Hamzah, N. Abbasizadeh, A. Najafinezhad, M. Kashefian, Synthesis of novel nanostructured bredigite–amoxicillin scaffolds for bone defect treatment: cytocompatibility and antibacterial activity. J. Sol-Gel. Sci. Technol. (2018). https://doi.org/10.1007/s10971-018-4606-1
42. F. Zheng, S. Wang, S. Wen, M. Shen, M. Zhu, X. Shi, Characterization and antibacterial activity of amoxicillin-loaded electrospun nano-hydroxyapatite/poly(lactic-co-glycolic acid) composite nanofibers. Biomaterials **34**(4), 1402–1412 (2013)
43. Z. Tabia, K. El Mabrouk, M. Bricha, K. Nouneh, Mesoporous bioactive glass nanoparticles doped with magnesium: drug delivery and acellular in vitro bioactivity. RSC Adv. **9**, 12232–12246 (2019)
44. S. Amudha, J. Ramana Ramya, K. Thanigai Arul, A. Deepika, P. Sathiamurthi, B. Mohana, K. Asokan, C.-L. Dong, S. Narayana Kalkura, Enhanced mechanical and biocompatible properties of strontium ions doped mesoporous bioactive glass. Composites B **196**, 108009 (2020)
45. N.A. Peppas, B. Narasimhan, Mathematical models in drug delivery: How modeling has shaped the way we design new drug delivery systems. J. Control. Release **190**, 75–81 (2014)
46. X. Wang, G. Wang, Y. Zhang, Research on the biological activity and doxorubicin release behavior in vitro of mesoporous bioactive SiO2-CaO-P2O5 glass nanospheres. Appl. Surf. Sci. **419**, 531–539 (2017). https://doi.org/10.1016/j.apsusc.2017.05.078
47. S. Shruti, A.J. Salinas, E. Ferrari, G. Malavasi, G. Lusvardi, A.L. Doadrio, L. Menabue, M. Vallet-Regi, Curcumin release from cerium, gallium and zinc containing mesoporous bioactive glasses. Microporous Mesoporous Mater. **180**, 92–101 (2013)
48. H.A. Merchant, H.M. Shoaib, J. Tazeen, R.I. Yousuf, Once-daily tablet formulation and in vitro release evaluation of cefpodoxime using hydroxypropyl methylcellulose: a technical note. AAPS Pharmscitech. **7**(3), E178–E183 (2006)
49. A.M. El-Kady, M.M. Ahmed, B.M. Abd El-Hady, A.F. Ali, A.M. Ibrahim, Optimization of ciprofloxacin release kinetics of novel Nano-bioactive glasses: Effect of glass modifier content on drug loading and release mechanism. J. Non-Cryst. Solids. **521**, 119471 (2019)
50. A.M. El-Kady, N.A. Kamel, M.M. Elnashar, M.M. Farag, Production of bioactive glass/chitosan scaffolds by freeze-gelation for optimized vancomycin delivery: effectiveness of glass presence on controlling the drug release kinetics. J Drug Deliv Sci Technol **66**, 102779 (2021). https://doi.org/10.1016/j.jddst.2021.102779